Compositional Grading for Efficient and Narrowband Emission in CdSe-Based Core/Shell Nanoplatelets

Author(s):
Rossinelli, Aurelio; Rojo, Henar; Mule, Aniket S.; Aellen, Marianne; Cocina, Ario; De Leo, Eva; Schäublin, Robin; Norris, David J.

Publication date:
2019

Permanent link:
https://doi.org/10.3929/ethz-b-000383045

Originally published in:
Chemistry of Materials 31(22), https://doi.org/10.1021/acs.chemmater.9b04220

Funding acknowledgement:
165559 - Optical Strong Coupling in Colloidal Quantum Dots (SNF)
339905 - Quantum-Dot Plasmonics and Spasers (EC)

Compositional Grading for Efficient and Narrowband Emission in CdSe-Based Core/Shell Nanoplatelets

Aurelio A. Rossinelli,[†] *Henar Rojo,*[†] *Aniket S. Mule,*[†] *Marianne Aellen,*[†] *Ario Cocina,*[†] *Eva De Leo,*[†] *Robin Schäublin,*[‡] *and David J. Norris**[,†]

[†] Optical Materials Engineering Laboratory, Department of Mechanical and Process Engineering, ETH Zurich, 8092 Zurich, Switzerland

[‡] Laboratory of Metal Physics and Technology, Department of Materials, ETH Zurich, 8092 Zurich, Switzerland

ABSTRACT. Colloidal semiconductor nanoplatelets exhibit exceptionally narrow photoluminescence spectra. This occurs because samples can be synthesized in which all nanoplatelets share the same atomic-scale thickness. As this dimension sets the emission wavelength, inhomogeneous linewidth broadening due to size variation, which is always present in samples of quasi-spherical nanocrystals (quantum dots), is essentially eliminated. Nanoplatelets thus offer improved, spectrally pure emitters for various applications. Unfortunately, due to their non-equilibrium shape, nanoplatelets also suffer from low photo-, chemical, and thermal stability, which limits their use. Moreover, their poor stability hampers the development of efficient synthesis protocols for adding high-quality protective inorganic shells, a well-known strategy to improve the performance of quantum dots. Herein, we report a general synthesis approach to highly emissive and stable core/shell nanoplatelets with various shell compositions, including CdSe/ZnS, CdSe/CdS/ZnS, CdSe/$Cd_xZn_{1-x}S$, and CdSe/ZnSe. Motivated by previous work on quantum dots, we find that slow, high-temperature growth of shells containing a compositional gradient reduces strain-induced crystal defects and minimizes the emission linewidth while maintaining good surface passivation and nanocrystal uniformity. Indeed, our best core/shell nanoplatelets (CdSe/$Cd_xZn_{1-x}S$) show photoluminescence quantum yields of 90% with linewidths as low as 56 meV (19.5 nm at 655 nm). To confirm the high quality of our different core/shell nanoplatelets for a specific application, we demonstrate their use as gain media in low-threshold ring lasers. More generally, the ability of our synthesis protocol to engineer high-quality shells can help further improve nanoplatelets for optoelectronic devices.

INTRODUCTION

Photoluminescence, the process by which a material absorbs and re-emits light, is critical for many photonic and optoelectronic devices. Consequently, highly luminescent semiconductor nanocrystals have been developed for applications such as solid-state lighting, displays, and lasers.[1-5] When a nanocrystal absorbs a photon, an electron–hole pair (or exciton) is created whose energy is affected by the nanocrystal boundary. Electron–hole recombination can then lead to the emission of a photon with a wavelength tunable via nanocrystal size and shape. State-of-the-art nanocrystals have been designed to exploit this effect and exhibit efficient luminescence in different wavelength ranges.[6] Arguably, the most studied nanocrystals have been those with a quasi-spherical shape, particles known as colloidal quantum dots (QDs). However, even after several decades of development, the best QD samples still exhibit a size distribution. This leads to spectral broadening in the absorption and emission characteristics, affecting performance in nanocrystal-based devices.

This broadening can be significantly reduced in a newer class of semiconductor nanocrystals known as nanoplatelets (NPLs). These particles have a thin rectangular shape with a uniform thickness of only a few atomic monolayers and lateral sizes of ~10 to 100s of nanometers.[7-8] In the case of CdSe NPLs, the thickness is sufficiently small that photoexcited electron–hole pairs are strongly confined in this one dimension.[9] The optical properties are then governed by this thickness. If the lateral sizes are above 10 nm, variations in these other two dimensions have negligible impact.[10] Also, because samples can be prepared in which all NPLs have the exact same thickness (e.g., 4 monolayers), NPLs can provide narrower absorption and emission lines than QDs. Thus, they offer color purity for lighting and displays, and enhanced gain for lasers.[11-12]

However, as prepared, NPLs are less photostable[13] and exhibit a lower photoluminescence quantum yield (QY) than state-of-the-art QDs. The fluorescence of NPLs is also highly sensitive to their geometry[14] and chemical environment.[15] The best QDs exploit “core/shell” structures, in which a layer of another material is deposited to protect the exciton from the surface and reduce the interaction with surface trap states and the surrounding matrix.[6] Moreover, protocols for growing a shell on the QD core have been continually improved and high-quality core/shell nanocrystals can now be produced for a large variety of shell types.[4,16-18] Such protocols typically utilize extended reaction times, high reaction temperatures, and customized precursor and ligand combinations. This allows for the epitaxial growth of uniform crystalline shells with a smooth core/shell interface, good surface passivation, and near-unity QYs.

For NPLs, however, core/shell structures of such high quality with simultaneously stable, efficient, and narrow emission have been more challenging to synthesize. The small thickness and anisotropic shape of NPLs lead to a lower thermodynamic stability compared to QDs.[19] This renders them prone to dissolution at elevated temperatures, making high-temperature shell growth difficult. As an alternative approach, colloidal atomic layer deposition (c-ALD) at low temperature can be used

to grow shells.[20-21] This method allows for a wide range of possible core/shell combinations and avoids issues related to low thermal stability. Unfortunately, the resulting NPLs typically show relatively low QYs, and their synthesis requires many purification steps, essentially one after each atomic layer is added to the shell.

A few protocols do exist that employ a continuous growth of the shell at relatively low temperatures. While such core/shell NPLs achieved QYs up to 80%, they suffer from limited reproducibility, and non-uniform and defective shell growth that broadens the emission.[22-24] Presumably, these limitations are a result of the synthesis being performed at lower temperatures. Meeting the fundamental challenges associated with the stability of NPLs at high temperature may allow new and improved core/shell NPLs with higher QYs, uniformity, and stability to be obtained.

To move in this direction, we recently succeeded in growing CdS shells on CdSe NPLs at high temperatures.[25] By improving the thermal stability of CdSe NPLs with the addition of cadmium oleate, we minimized the NPL dissolution at high temperature and obtained uniform and bright core/shell NPLs with narrow emission linewidths. (Since our work appeared, an alternative high-temperature approach, in which NPL cores are injected into the growth solution at high temperature, has also been reported, but without QY values.[26]) In principle, our approach could also be applied to other shell types to create core/shell NPL structures with improved and tailored optical and electronic properties. However, a deeper understanding of the shell growth on such quasi-two-dimensional (quasi-2D) nanoplatelets is necessary to develop robust and efficient synthesis protocols.

In the following, we address this need by investigating the high-temperature growth of a variety of shells on CdSe nanoplatelets. In particular, our synthesis protocol allows us to explore core/shell structures that have been well investigated in CdSe QDs.[16-17,27-29] First, we discuss the effect of strain in CdSe/ZnS core/shell NPLs and elucidate the limitations of ZnS in providing a uniform shell morphology for narrow emission linewidths. Our conclusions are verified by introducing a bridging layer of CdS between CdSe and ZnS. Second, to reduce the emission linewidth and improve the QY, we develop optimized CdSe/$Cd_xZn_{1-x}S$ core/shell NPLs with a compositionally graded shell. Such core/shell NPLs exhibit high particle crystallinity and uniformity, narrow emission linewidths, and high QYs. We discuss the improved quality and characterize the structural and optical properties of these graded core/shell NPLs. Finally, we demonstrate the general flexibility of our coating protocol by synthesizing core/shell NPLs with a ZnSe shell. We conclude with a demonstration of the utility of our core/shell NPLs by examining their use in all-NPL ring lasers.

RESULTS AND DISCUSSION

CdSe/ZnS Core/Shell NPLs. As mentioned above, we previously developed a high-temperature protocol for the addition of uniform CdS shells to CdSe NPLs.[25] However, the imperfect protection of the exciton by the CdS shell can be a limiting factor for the photoluminescence efficiency of CdSe/CdS

core/shell NPLs. One potential solution is to exploit a larger-bandgap material for the shell. The exciton is then more strongly confined to the core, and any effects of an incomplete surface passivation can be reduced.[30] This was recently implemented by synthesizing highly luminescent CdSe/ZnS NPLs.[24,31] However, the efficient photoluminescence in CdSe/ZnS NPLs came with broadening of the emission linewidth and an irregular shell growth. Our first goal was to study these problems and see if they could be avoided to obtain high-quality ZnS shells.

Therefore, we synthesized CdSe/ZnS core/shell NPLs by modifying our previously reported high-temperature protocol for CdS shells. The final particles, which resulted from the detailed studies described in the next paragraphs, are shown in Figure 1a. To achieve this result, an approach to minimize the interfacial strain was employed. Otherwise, shape irregularities would emerge. For instance, we found that while thin ZnS shells could form a relatively uniform surface, indicative of controlled epitaxial shell growth, irregular shells arose with increasing ZnS thickness (see Figure S1 in the Supporting Information). This is expected as CdSe and ZnS have a large lattice mismatch (~12%). Furthermore, NPLs have a flat and significantly larger surface than QDs. As a result, increased strain with thicker ZnS shells can be released by forming defects in the shell.[32-34]

Our approach to minimize the interfacial strain and the resulting shape irregularities was to modify the structure and alloy the interface. For this purpose, we reduced the initial precursor concentration and increased the monomer solubility. We added only 25% of the total amount of $Zn(OA)_2$ at the beginning of the reaction and injected the remaining part along with 1-octanethiol at 300 °C. Furthermore, we injected oleic acid (OA) together with 1-octanethiol. This excess of OA was necessary to avoid the formation of irregularly shaped shells (Figure S2). It is well known that OA increases the monomer solubility and reduces the growth rate.[35] Under these adjusted synthesis conditions, we avoided the irregular shell growth and could reduce the emission linewidth (Figure S3). The core/shell structure was then analyzed by high-angle annular dark-field scanning transmission electron microscopy (HAADF STEM) and energy-dispersive X-ray spectroscopy (EDS) (Figure 1a and Figure 2). We measured a shell thickness of 1–1.5 nm, which is smaller than for CdSe/CdS NPLs using the same amount of precursor. The EDS analysis (Figure 2) reveals the presence of Cd and Se in both the core as well as the inner part of the shell. Partly, this can be explained by diffusion. At such high reaction temperatures cation diffusion is enhanced,[36] which can lead to alloying of Cd and Zn at the core/shell interface. In contrast, anion diffusion is substantially slower, and we do not observe strong anion diffusion into the shell of CdSe/CdS NPLs synthesized under the same conditions. However, a reduction of the lateral size of CdSe/ZnS NPLs (~150 nm^2) compared to the CdSe NPL seeds (~210 nm^2) can be observed. We believe that the smaller lateral size results from a prolonged initial etching of the CdSe NPLs due to the slower growth rate. The subsequent incorporation of this dissolved material into the shell enhances interfacial alloying and explains the detection of Cd and Se in the shell. This is further supported by the relative concentrations of Cd and Zn in these core/shell

NPLs. Despite a shell thickness of 1–1.5 nm, and thus a larger volume of the shell compared to the core, our EDS analysis shows a ratio Zn:Cd of only ~0.73:1. Such a small ratio can be achieved only if the shell contains Cd from a partial dissolution of the core.

These experiments also indicate that the use of Zn(oleate)$_2$ [Zn(OA)$_2$] instead of Cd(oleate)$_2$ [Cd(OA)$_2$] as the cation precursor affects the etching of the NPLs prior to shell growth. To examine this effect, we monitored the absorption spectrum and the shape of CdSe NPLs while heating to 300 °C with either Cd(OA)$_2$ or Zn(OA)$_2$. In the presence of Zn(OA)$_2$, an increased broadening of the lowest-energy excitonic peak and an emergent absorption at wavelengths longer than the NPL excitonic features can be observed (Figure S4). An analysis of the corresponding HAADF STEM images shows no significant difference in the average lateral size at high temperatures (Figures S5 and S6). However, these images reveal a substantial change in the shape at high temperatures. In the presence of Cd(OA)$_2$, the NPLs dissolve slowly and morph into uniform circular disks. In contrast, Zn(OA)$_2$ enhances the facet-specific dissolution towards non-uniform shapes. Furthermore, a higher signal intensity was recorded in HAADF STEM at the edges of the NPLs that were treated in Zn(OA)$_2$ at high temperature, indicating an increased thickness. This irregular material transfer to the edges can explain the increased absorption at longer wavelengths and the broader excitonic features measured for these aliquots. Such an anisotropic material transfer induced by Zn(OA)$_2$ has also been observed previously on other nanocrystals.[37] We conclude that a combination of high strains in CdSe/ZnS NPLs and the anisotropic etching had induced the previously observed emission broadening and irregular shell morphology. By adjusting the shell growth conditions, these effects could be reduced in CdSe/ZnS NPLs (Figure 1a).

CdSe/CdS/ZnS Core/Shell/Shell NPLs. To test this understanding further, we coated CdSe NPLs with CdS before the growth of ZnS. In this heterostructure, CdS reduces strain by bridging the lattice mismatch between CdSe and ZnS. Indeed, for QDs such a shell structure resulted in better optical properties, while maintaining relatively narrow emission linewidths of 77 meV (24 nm at ~620 nm).[17] In addition, for NPLs the use of Cd(OA)$_2$ as the precursor for the CdS shell growth avoids the anisotropic etching of the CdSe core. To obtain CdSe/CdS/ZnS NPLs, we coated CdSe NPLs first with CdS by the slow injection of 1-octanethiol at 300 °C into a mixture of CdSe NPLs and Cd(OA)$_2$. This step was then followed by a second slow injection of 1-octanethiol and Zn(OA)$_2$ at 280 °C. Figure 1b shows a HAADF STEM image of such CdSe/CdS/ZnS NPLs. They have a uniform morphology with a shell thickness of approximately 2–3 nm. Interestingly, we noticed an improved colloidal stability of the final core/shell/shell NPLs after the addition of ZnS. This suggests that the ligands are bound more strongly on the NPLs capped with ZnS than CdS.[38] After the ZnS overcoating, we also measured an increase in the QY from 60–70% in CdSe/CdS NPLs up to ~80% in CdSe/CdS/ZnS NPLs.

CdSe/Cd$_x$Zn$_{1-x}$S Core/Shell NPLs. The above data demonstrate the advantage of combining CdS and ZnS in the shell and indicate the dual benefit of strain reduction and improved surface

passivation. It also suggests that the ideal shell would contain a gradual increase in concentration of ZnS towards the surface. We therefore designed a synthesis protocol for a compositionally graded alloyed shell with a Cd-rich inner part and a Zn-rich outer part. It has been shown that cadmium chalcogenides grow on CdSe at a higher rate than the corresponding zinc chalcogenides.[39-40] This difference in the reaction rates enabled us to obtain the desired composition gradient by combining CdSe NPLs with $Cd(OA)_2$ and $Zn(OA)_2$ in different ratios. The shell synthesis was performed at 300 °C by slowly injecting 1-octanethiol together with oleic acid. Figure 1c shows such CdSe/$Cd_xZn_{1-x}S$ core/shell NPLs using a $[Cd(OA)_2]$: $[Zn(OA)_2]$ precursor ratio of 1:2. This approach resulted in crystalline and uniform shells with a thickness of 1.5–2 nm. Compared to the original synthesis of CdSe/CdS NPLs, nearly no formation of side products was observed. We attribute this reduced homogeneous nucleation to a higher monomer solubility due to the injection of oleic acid and the lower reactivity of the Zn-precursor.[35,40] We discuss the optimization and characterization of CdSe/$Cd_xZn_{1-x}S$ core/shell NPLs further in a later section.

CdSe/ZnSe Core/Shell NPLs. In principle, such a graded composition can be synthesized also with other shell materials. However, to the best of our knowledge, protocols for coating NPLs with a uniform shell have so far been limited to sulfide shells. By synthesizing novel shell types, the available core/shell NPL systems can be extended, which allows additional control over the NPL properties. We therefore examined ZnSe as an additional shell material. Because the lattice mismatch between CdSe and ZnSe (~6%) lies between the values for CdSe–CdS (~4%) and CdSe–ZnS (~12%) , we expected to benefit from compositional grading but have a more uniform shell growth than for CdSe/ZnS NPLs.

For the Se precursor, we used a solution of Se dissolved in 1-octadecene (Se-ODE). To obtain CdSe/ZnSe core/shell NPLs, we then slowly injected Se-ODE together with oleic acid at different temperatures between 260 and 300 °C into a mixture of CdSe NPLs and $Zn(OA)_2$. Because Se-ODE exhibited higher reactivity than 1-octanethiol (the sulfur precursor used above), the control of the shell growth was more challenging, and we observed substantial homogeneous nucleation of ZnSe nanocrystals. Figure 1d shows the NPLs resulting from the synthesis at 300 °C. We measured a shell thickness of 2–3 nm in these CdSe/ZnSe NPLs, which is slightly larger than for NPLs with ZnS shells. This faster growth can be attributed to a higher reactivity of Se-ODE compared to 1-octanethiol, leading to a faster and more complete precursor conversion.

When the composition was analyzed by EDS, the Cd was found in the shell despite the absence of Cd as a precursor during the shell growth (Figure S7). Similar to the case of ZnS shells, this may be explained by a partial dissolution of the CdSe NPL cores and the subsequent incorporation of this material into the shell (see Section S1 in the Supporting Information). Furthermore, since only the cation is altered between core and shell, the high reaction temperature is expected to accelerate the cationic diffusion near the core/shell interface.[36]

X-Ray-Diffraction (XRD) Analysis. XRD results can complement the characterization of the crystal structure performed by electron microscopy. All of our core/shell NPLs show zinc blende (zb) diffraction peaks, indicating that the shell adopts the crystal structure of the core (Figure 3). (Data for the initial CdSe NPL cores are provided in Figure S8.) Among the core/shell NPLs, differences in the peak width and shape can be observed. While the CdSe/CdS/ZnS NPLs show the narrowest diffraction signals, the peaks broaden substantially in the CdSe/ZnS NPLs. Partially, this is caused by the difference in lateral size and thickness of the NPLs, which affects the Scherrer line broadening. However, strain in the core/shell NPLs also contributes to the peak broadening. CdSe has a larger lattice constant than the material in the shell. Thus, a higher content of Zn and/or S in the shell strains the NPLs more. This results in a spread of the diffraction angles and broadens the pattern.

In addition, the core/shell structure also affects the symmetry of the diffraction peaks. The larger lattice constant in the core contributes to the diffraction signal at smaller angles. However, the smaller volume of the core compared to the shell reduces its contribution to the pattern and explains the observed asymmetry of the diffraction peaks [most obvious for the (220)-reflections of CdSe/$Cd_xZn_{1-x}S$ and CdSe/ZnS NPLs near 43°]. Furthermore, biaxial strain in the core/shell NPLs owing to the quasi-2D geometry of the core may increase the peak asymmetry.[41]

Optical Characterization of Core/Shell NPLs. The influence of the shell composition on the emission was characterized by absorption and emission spectroscopy (Figure 4). We achieved narrow emission linewidths below 60 meV [full-width-at-half-maximum (FWHM)] for our core/shell NPLs. While this value is broader than the initial CdSe NPL cores (38 meV, 8.1 nm; see Figure S8), it is significantly lower than state-of-the-art QDs (77 meV).[17] The smallest values were measured for graded CdSe/$Cd_xZn_{1-x}S$ core/shell NPLs (56 meV, Table 1). For 4-monolayer-thick-CdSe/$Cd_xZn_{1-x}S$ NPLs emitting at 655 nm, this linewidth corresponds to a 19.5 nm FWHM (Table 1). Of our different optimized NPLs, only CdSe/ZnS core/shell NPLs showed a significantly broader emission peak with a FWHM of ~76 meV (~23.7 nm at 620 nm, Table 1).

For CdSe/CdS/ZnS NPLs we measured emission wavelengths centered at 660–670 nm. Slightly shorter values were obtained for CdSe/$Cd_xZn_{1-x}S$ NPLs where we measured 655 nm for a precursor ratio of $Cd(OA)_2$: $Zn(OA)_2$ = 1:2. This can be attributed to a small difference in the shell thickness and a different Cd content in the shell. Reducing Cd (in favor of Zn) increases the exciton confinement, which leads to emission at shorter wavelengths. Hence, the shortest values were measured for CdSe/ZnS NPLs at ~620 nm for smooth ZnS shells. We also observed an increase in the photoluminescence lifetime with higher Cd content in the shell (Figure S9 and Table 1).

Interestingly, CdSe/ZnS NPLs with shells synthesized at room temperature by c-ALD emit at wavelengths shorter than 600 nm, even with thicker shells.[24] This implies a structural difference in the shell or at the interface. The incorporation of material from the core into the shell for our CdSe/ZnS NPLs (as observed by EDS, Figure 2) can explain the more pronounced red-shift that we observe. For

example, more Cd in the shell increases the exciton delocalization. Consequently, for our CdSe/ZnS NPLs that have an irregular shell morphology, emission occurred near 610 nm (Figure S3).

Our CdSe/ZnSe NPLs showed an emission highly sensitive to the reaction temperature. Emission wavelengths were measured from ~630 to 685 nm with the longest values obtained for reactions performed at the highest temperature of 300 °C. Notably, such a large emission red-shift of 170 nm (0.6 eV) was achieved while retaining narrow emission having a FWHM of only 22 nm (59 meV, Table 1). We explain this emission red-shift with the high reaction temperature that accelerates both the partial dissolution of the CdSe NPL core followed by its incorporation into the shell and the cation diffusion near the core/shell interface. This results in a reduction of the potential well in the inner part of the shell and enhances the delocalization of the exciton wave function.

Optimization of CdSe/$Cd_xZn_{1-x}S$ Core/Shell NPLs. To understand the properties of the $Cd_xZn_{1-x}S$ shells, we examined the synthesis of these materials further. As discussed above, the spectral position of the emission can be controlled by tuning the ratio between Cd and Zn. Thus, we prepared core/shell NPLs using different cation precursor ratios and precursor quantities. The molar fraction of $Cd(OA)_2$ (relative to the total amount of metal oleate) was varied between 0 and 100%. Reactions were then performed with a total precursor amount (Cd plus Zn) of 0.05, 0.1, and 0.2 mmol metal oleates (the molar ratio between metal oleates and 1-octanethiol was fixed at 1:1.2). The results show that a larger amount of total precursor led to a stronger emission red-shift (Figure 5a). This is expected for the formation of a thicker shell and, therefore, weaker exciton localization. The emission wavelength is also clearly dependent on the precursor ratio. Increasing the fraction of $Cd(OA)_2$ up to around 25–30% shifts the emission steadily towards longer wavelengths. However, in all concentration series we observed no further red-shift beyond a $Cd(OA)_2$ fraction of 30%. This indicates that a relatively large fraction of $Zn(OA)_2$ is required to achieve changes in the shell composition and, hence, the emission behavior. In fact, for a Cd:Zn precursor ratio of 1:2 we measured a concentration ratio Cd:Zn of 3.88:1 in the final core/shell NPLs by Rutherford back scattering (RBS) (Figure S10a). Subtracting the material in the CdSe core (Cd:Se ratio of 1.30:1, Figure S10b) results in a Cd:Zn ratio of ~2.8:1 in the shell.

The data show that the precursor ratio and the final shell thickness also affect the emission linewidth (Figure 5b,c). Adding only $Zn(OA)_2$ broadens the emission with increasing shell thickness. This differs from observations in QDs, where the growth of ZnS shells on CdSe has only little effect on the emission linewidth.[42] In contrast, the addition of more $Cd(OA)_2$, either by adding more precursor or increasing the Cd:Zn molar ratio, results in narrower emission peaks, reaching linewidths below 60 meV (FWHM). This value corresponds to those measured for CdSe/CdS core/shell NPLs obtained via the c-ALD approach (shaded area in Figure 5b) in which the shell is expected to grow with atomic precision.[20-21] Thicker shells also minimize variations in the emission linewidth, as indicated in Figure 5c by the encircled clusters of black and red data points for reactions with

[$Cd(OA)_2$] ≥ 25%. Our linewidth narrowing can be explained by an improved shell uniformity achieved for thicker shells (as observed in pure CdS shells[25]) and reduced strains and defects.[42] Strains due to an increased lattice mismatch explain also the broader emission with linewidths up to 100 meV for the syntheses of ZnS shells at a higher precursor concentration. (As discussed above, this leads to the formation of irregular shell morphologies.) No clear trend could be observed for the reaction series with 0.05 mmol metal oleate. In such thin shells, strain plays a smaller role and we can obtain even narrower emission linewidths with ZnS than with CdS shells. Instead, the stronger exciton confinement with thinner shells renders the linewidth more sensitive to synthesis conditions and its spread becomes generally larger.

Structural and Optical Characterization of CdSe/$Cd_xZn_{1-x}S$ Core/Shell NPLs. We expect that the simultaneous addition of $Cd(OA)_2$ and $Zn(OA)_2$ at the beginning of the shell synthesis allows the formation of epitaxial, compositionally graded $Cd_xZn_{1-x}S$ shells. To verify this, we performed a detailed structural analysis of these core/shell NPLs. Figure 6a shows a cross-sectional view of a CdSe/$Cd_xZn_{1-x}S$ NPL along the [100]-direction at atomic resolution acquired by STEM. The image shows that the shell adopts the lattice of the core, forming an epitaxial interface. The heavier and brighter core can be distinguished clearly from the shell due to the difference in composition. In addition, the elemental profile of such core/shell NPLs can be obtained by EDS for top and side views (Figure 6b). Figure 6c shows the elemental concentration profile across a stack of 4 NPLs, observed from the side. The profile is extracted in the direction of the white arrow in Figure 6b. It reveals a spatially dependent Zn concentration, increasing with the distance from the CdSe core. Hence, these data are consistent with the formation of an epitaxial and compositionally graded shell.

Combining this structural information with the resulting optical properties allows one to draw conclusions for the design of optimized core/shell NPLs. In particular, besides the effect on the emission linewidth we further evaluated the impact of the shell design on the QY, a key quantity for many applications. Figure 7a shows the QY as a function of excitation wavelength for CdSe/$Cd_xZn_{1-x}S$ NPLs for which the shell was grown with a precursor ratio [$Cd(OA)_2$] : [$Zn(OA)_2$] of 1:2. These NPLs exhibited narrow emission while containing a relative high amount of Zn in the outer part of the shell. A very high QY of 90% that is nearly independent of the excitation wavelength was achieved without additional surface treatment after the synthesis.

The data suggest that the high QY values observed for these graded shells result from several factors. First, the presence of a ZnS-rich outer layer improves the passivation and protection from the environment compared to a pure CdS shell. This can explain why we measured lower QY values (60–70%) for our CdSe/CdS NPLs. Similarly, incomplete surface passivation may also be limiting the QY of our CdSe/ZnSe NPLs, for which we measured values near 50% (Table 1). We expect that an increase of the QY for CdSe/ZnSe NPLs may be possible with an improved surface passivation, possibly by adding ZnS or a better ligand coverage. The second factor that can lead to high QY in our

optimized $Cd_xZn_{1-x}S$ shells is their high Cd content in the part of the shell close to the core/shell interface. Compared with a pure, unalloyed ZnS shell, this reduces the lattice mismatch and minimizes defect formation, allowing a narrow emission peak with high QY to be obtained. (We assume that the reported high QY values in CdSe/ZnS NPLs[31] also result from partial alloying at the interface.) The third factor is the high reaction temperature and slow shell growth, which can reduce lattice strain and defects by atomic diffusion.[43-44] A similar behavior was observed in CdSe/CdS nanorods, where a slow over-coating of the initially slightly defective shell at high temperatures allowed for an increase of the QY to near unity.[45]

To confirm the emission stability of our CdSe/$Cd_xZn_{1-x}S$ NPLs we recorded the photoluminescence of NPLs excited at different wavelengths (400 to 640 nm, Figure S11a) and fluences (10 to 1000 μJ/cm^2, Figure S11b). The core/shell NPLs show a stable emission peak that is nearly independent of the excitation wavelength and power, even for the highest fluences.

To this point, all of our initial CdSe NPL cores have been 4-monolayers (4-ML) thick. Because the direct synthesis of thicker 6-monolayer-thick (6-ML) CdSe NPLs has also recently been reported,[46-47] we tested the versatility of our shell protocol and applied it to these NPLs (Figure S12). The resulting CdSe/$Cd_xZn_{1-x}S$ core/shell NPLs showed a narrow emission peak with a FWHM of 57 meV (22 nm) and a strong red-shift to 692 nm. The corresponding absorption and emission spectra, HAADF STEM images, and EDS data are shown in Figure 8. These core/shell NPLs exhibit very high QYs between 90 and 95% and exceptional emission stability (Figure 7b and Figure S11c,d). Hence, such compositionally graded CdSe/$Cd_xZn_{1-x}S$ core/shell NPLs reveal the benefit of strain reduction and surface passivation for improved optical performance.

Nanoplatelet Ring Lasers. The properties discussed above illustrate the potential of the core/shell NPLs for applications that rely on narrow emission with high QY. However, the suitability for more complex optical devices remains to be examined. Therefore, as a demonstration, we evaluated the performance of our different core/shell NPL structures for lasing applications.

In semiconductor nanocrystals, non-radiative Auger recombination can be a critical loss mechanism competing with population inversion and lasing.[48] However, it has been shown that Auger recombination can be significantly slowed by utilizing core/shell nanocrystals with compositionally graded core/shell interfaces.[49-50] In addition, the relaxation from 3D to 1D exciton confinement in NPLs may further reduce the Auger recombination rate by enforcing a stricter momentum conservation. In this context, NPLs have shown great potential as an active gain material for lasers. Low-threshold lasing under pulsed and continuous wave photoexcitation have recently been reported for bare CdSe NPLs and NPLs coated with a shell by c-ALD.[51-54] Core/shell NPLs with a compositionally graded shell may provide further improvements in performance, stability, and variability compared to bare NPLs.

For our evaluation, we chose ring resonators as a platform because of their simple architecture.[55] Namely, we used patterned films of core/shell NPLs that contained circular waveguides (Figure 9a,b). In this design, the NPLs create both the ring resonator and provide the gain material. We fabricated such structures by template-stripping films of core/shell NPLs from pre-patterned silicon templates.[56] As we showed previously for QDs,[56] this method allows for rapid production of structures with high quality and variable geometry. To achieve population inversion and lasing, the rings were then illuminated by ultrafast laser pulses at a wavelength of 405 nm. Figure 9c shows the resulting power-dependent emission spectra of a 4-monolayer-CdSe/$Cd_xZn_{1-x}S$ NPL ring laser. The transition from spontaneous emission to multimode lasing can be observed as an abrupt increase of the emission peak intensity and the appearance of a series of sharp lasing peaks (cavity modes) above a threshold of 13 μJ/cm^2 (Figure 9d,e). This threshold is lower than values measured for core/shell QDs using the same ring structures.[55] Our different core/shell NPL ring lasers all showed lasing modes at wavelengths between ~630 (CdSe/ZnS NPLs) and ~720 nm (6-monolayer-CdSe/$Cd_xZn_{1-x}S$ NPLs), and low threshold fluences below 50 μJ/cm^2 (Figure S13). Our analysis supports the potential of such core/shell NPLs for lasing applications. Despite the simple structure, we achieved low thresholds and stable lasing performance up to very high excitation powers. We were able to sustain lasing for excitation powers ranging over ~2 orders of magnitude. Future work on the influence of the shell structure on the Auger recombination rate may help optimize these core/shell NPLs further for lasing applications.

CONCLUSIONS

We have developed a high-temperature, slow-injection shell-growth protocol that can produce core/shell nanoplatelets with various shell designs. The structural and optical characterization of the resulting materials revealed the crucial role of a compositional gradient in nanoplatelet shells. Such a design helps avoid the formation of strain-induced defects in these anisotropic nanocrystals and enables high emission efficiencies and stability while retaining narrow emission linewidths. As a consequence, we achieved spectrally narrow and tunable emission, and reached QYs above 90%, overcoming previous limitations in NPL-based core/shell structures. In addition, such control over the shell composition helped us achieve low lasing thresholds in simple architectures with stable output over large power ranges. These core/shell NPLs can potentially impact applications relying on narrow, bright, efficient, and stable emission. Indeed, during the review process of this work very low optical gain thresholds and efficient LEDs have been shown for core/shell NPLs based on our high-temperature synthesis protocol.[57-58] Furthermore, owing to their unique geometry, such core/shell structures may be ideal for fundamental studies of diffusion processes, strain effects, and band-structure engineering in nanocrystals.

EXPERIMENTAL SECTION

Materials and Reagents. 1-octadecene (ODE, 90%, #O806), 1-octanethiol (≥98.5%, #471836), 2-propanol (≥99.9%, #34965), acetonitrile (≥99.9%, #34998), cadmium acetate hydrate [Cd(acetate)$_2$ hydrate, ≥99.99%, #229490], cadmium acetate dihydrate [Cd(acetate)$_2$ dihydrate, 98%, #289159], methyl acetate (≥98%, #W267600), cadmium chloride (technical grade, #655198), chloroform (99.8%, #132950), *n*-hexane (≥97.0%, #34859), methylcyclohexane (MCH, 99%, #M37889), myristic acid (≥98%, #70082), octane (98%, #412236), oleic acid (OA, 90%, #364525), selenium (≥99.5%, #209651), trifluoroacetic acid (≥99.0%, #302031), trifluoroacetic anhydride (≥99%, #106232), zinc acetate (99.99%, #383317), and zinc oxide (≥99.0%, #96479) were purchased from Sigma-Aldrich. Octadecyltrichlorosilane (ODTS, 96%) was purchased from Merck KGaA. Cadmium oxide (99.999%, #48-0800) was obtained from Strem Chemicals. Oleylamine (OAm, 80–90%, #129541000) and triethylamine (99%, #157910010) were acquired from Acros Organics. Methanol was purchased from Thommen-Furler AG and absolute ethanol from Alcosuisse AG. Four-inch diameter, single-side-polished, single-crystalline Si(100) wafers with <0.4 nm root-mean-square (RMS) roughness and thicknesses of either 500 or 1000 μm were purchased from Silicon Valley Microelectronics or Silicon Quest and diced into 2 × 2 cm^2 square pieces. All chemicals were used without further purification, except where noted.

Preparation of Cadmium Myristate [Cd(myristate)$_2$], Cadmium Oleate [Cd(oleate)$_2$], and Zinc Oleate [Zn(oleate)$_2$]. Cadmium carboxylates and zinc oleate were synthesized following a modified protocol by Hendricks et al.[59] Briefly, 5.75 g CdO (3.65 g ZnO) and 20 mL acetonitrile were mixed in a 100-mL round-bottom flask. The mixture was then stirred and cooled in an ice bath. Subsequently, 6.2 mL of trifluoroacetic anhydride, and 0.7 mL trifluoroacetic acid were added. After 10 min, the ice bath was removed and the flask heated at 50 °C until the solution turned clear. In a 500-mL Erlenmeyer flask, 180 mL 2-propanol, 14.0 mL of triethylamine, and 20.6 g myristic acid (or 28.6 mL oleic acid) were mixed and stirred. The warm cadmium trifluoroacetate (or zinc trifluoroacetate) solution was then slowly added to the myristic acid (or oleic acid) solution while stirring. The resulting white precipitate was vacuum-filtered using a fritted glass funnel and rinsed thoroughly with methanol. The final product was dried in a vacuum oven over night and stored under ambient conditions.

Preparation of Zinc Oleate Stock Solution. 367 mg Zn(acetate)$_2$, 7 mL ODE, and 1.2 mL OA were mixed in a glass jar in a N_2-filled glovebox. The mixture was then stirred at 220 °C for 2 h. Afterwards, it was allowed to cool to room temperature (RT). While cooling, 1.3 mL OAm was added at around 100 °C to prevent solidification. The final product was stored in a N_2-filled glovebox.

Preparation of Se-ODE Stock Solution. 79 mg Se powder (1 mmol) (stored in a N_2-filled glovebox) and 10 mL ODE was added to a 50-mL round-bottom flask and degassed at RT under vacuum for 30 min. The mixture was then heated to 240 °C under N_2 and kept for 30 min. Afterwards, it was allowed to cool to RT and transferred to a N_2-filled glovebox.

Synthesis of 4-Monolayer-Thick CdSe NPLs. For the CdSe NPL synthesis, 680 mg Cd(myristate)$_2$, 48 mg Se powder (stored in a N_2-filled glovebox), and 60 mL ODE were added to a 250-mL round-bottom flask and degassed at RT under vacuum for 30 min. Then, the mixture was heated to 240 °C under N_2. At 200 °C, 256 mg Cd(acetate)$_2$ dihydrate was added. The mixture was kept at 240 °C for 8–9 min. Afterwards, the reaction flask was cooled using an air gun to 160 °C. During this cooling step, 3 mL OA was added when the temperature reached 185 °C. Once at 130 °C, the flask was placed in a water bath and cooled to RT. Then, 10 mL hexane was added and the mixture was centrifuged at 8000 rpm (8586 g) for 10 min. The precipitate was re-dispersed in 20 mL hexane and kept undisturbed for 1 h. Afterwards, it was centrifuged at 7000 rpm (6574 g) for 7 min. Unwanted 3-monolayer-thick NPLs were removed as the precipitate. The 4-monolayer-thick NPLs in the supernatant were then precipitated from the hexane dispersion by adding methyl acetate and centrifuging at 6500 rpm (5668 g) for 3 min. The precipitate was re-dispersed in 6 mL hexane and stored in the dark under ambient conditions until needed. Optical and X-ray diffraction data are shown in Figure S8. We note that by convention an *m*-monolayer-thick CdSe NPL contains *m* atomic layers of Se and *m*+1 layers of Cd.

Synthesis of 6-Monolayer-Thick CdSe NPLs. The synthesis of 6-monolayer CdSe NPLs was adapted from Cho et al.[47] Briefly, 170 mg Cd(myristate)$_2$ and 14 mL ODE were mixed in a 100-mL round-bottom flask and degassed at 85 °C under vacuum for 30 min. Then, the mixture was heated up to 250 °C under N_2. At 250 °C, 12 mg Se powder (stored in a N_2-filled glovebox) dispersed in 1 mL ODE was quickly injected (the dispersion was sonicated for 20 min). 20 s later, 60 mg Cd(acetate)$_2$ hydrate was added. After 1 min, 0.15 mL aqueous $CdCl_2$ solution (0.5 M) was added dropwise over a period of 90 seconds. The mixture was then kept for an additional 6 min at 250 °C. Afterwards, the reaction flask was cooled to RT using an air gun. During this cooling step, 2 mL OA mixed with 15 mL MCH was added slowly when the temperature reached 180 °C. For the purification, the mixture was first centrifuged for 10 min at 8500 rpm (9693 g). The precipitate was re-dispersed in 1.5 mL MCH and centrifuged at 6500 rpm (5668 g) for 2 min. Salts and aggregated NPLs were removed as the precipitate. 3 mL hexane and 6 mL methyl acetate were then added to the 6-monolayer-thick NPLs in the supernatant and the mixture was centrifuged at 8000 rpm (8586 g) for 7 min. The precipitate was re-dispersed in 1 mL hexane and stored in the dark under ambient conditions until needed. A stable reaction temperature is necessary for a high yield of 6-monolayer-thick NPLs. Otherwise, unwanted 5-monolayer-thick NPLs that form during the synthesis can be removed selectively as precipitate by centrifuging the final dispersion at 8000 rpm (8586 g) for 30 min. Optical and STEM data are shown in Figure S12.

Synthesis of CdSe/$Cd_xZn_{1-x}S$ Core/Shell NPLs. In a typical synthesis, 4-monolayer CdSe NPLs [an amount equivalent to 1 mL of NPL dispersion with an optical density (OD) of 120 at the lowest energy excitonic peak, assuming a 1-cm optical path length], 10 mL ODE, 400 µL OA, 90 mg

$Cd(oleate)_2$ and 167.5 mg $Zn(oleate)_2$ (total of 0.4 mmol metal oleate, molar ratio of 1:2) were added to a 100-mL round-bottom flask. The mixture was degassed under vacuum for 35 min at RT and 15 min at 80 °C. Afterwards, 2 mL OAm (stored in a N_2-filled glovebox) was added and the temperature was raised to 300 °C under N_2 at a rate of ~15 °C/min. Starting at 165 °C, a solution of 83 µL 1-octanethiol (0.48 mmol) dissolved in 7 mL ODE and 2 mL OA was injected at a rate of 4.5 mL/h. After complete injection, the solution was kept at 300 °C for 40 min. Subsequently, the product was cooled down, and, at 40 °C, ~5 mL hexane was added.

The core/shell NPLs were purified by selective precipitation. In a first step, the mixture was centrifuged at 6500 rpm (5668 g) for 6 min. The core/shell NPLs in the precipitate were re-dispersed in 5 mL hexane. [If a significant amount of core/shell NPLs remained in the supernatant after this centrifugation step, they can be precipitated by adding methyl acetate and centrifuging at 6500 rpm (5668 g).] Then, ~5 mL methyl acetate was added to the dispersion of core/shell NPLs in hexane until the mixture turned turbid and it was centrifuged at 6500 rpm (5668 g) for 10 min. This process (i.e. dispersion of the NPLs in hexane followed by precipitation with methyl acetate) was repeated. The core/shell NPLs were then re-dispersed in 3 mL hexane and centrifuged at 6500 rpm (5668 g) for 7 min to separate the stable core/shell NPLs in the supernatant from aggregated core/shell NPLs. The core/shell NPLs in the supernatant were then filtered using a 0.2 µm pore-size polytetrafluoroethylene (PTFE) membrane filter and stored in the dark under ambient conditions.

The above synthesis can be performed using different ratios of $Cd(oleate)_2$ to $Zn(oleate)_2$ keeping the added amount of metal oleate constant. In general, a higher Zn:Cd ratio leads to a slight improvement of the colloidal stability of the final core/shell NPLs. For pure $Cd(oleate)_2$, CdS is formed as a side product.[25] This side product can be efficiently removed by increasing the amount of hexane added upon cooling of the reaction product and the subsequent purification steps.

The quality of the resulting core/shell nanoplatelets is improved if the temperature ramp from 80 °C to the reaction temperature of 300 °C is slowed down at around 270 °C, and reaches 300 °C after ~30 min.

Synthesis of CdSe/CdS/ZnS Core/Shell/Shell NPLs. In a typical synthesis, 4-monolayer CdSe NPLs [an amount equivalent to 1 mL of NPL dispersion with an optical density (OD) of 120 at the lowest energy excitonic peak, assuming a 1-cm optical path length], 10 mL ODE, 400 µL OA, and 270 mg $Cd(oleate)_2$ (0.4 mmol) were added to a 100-mL round-bottom flask. The mixture was degassed under vacuum for 35 min at RT and 15 min at 80 °C. Afterwards, 2 mL OAm (stored in a N_2-filled glovebox) was added and the temperature was raised to 300 °C under N_2 at a rate of ~15 °C/min. Starting at 165 °C, a solution of 83 µL 1-octanethiol (0.48 mmol) dissolved in 9 mL ODE was injected at a rate of 4.5 mL/h. After complete injection, the solution was cooled to 200 °C, 2 mL OA (stored in a N_2-filled glovebox) was added, and the mixture was kept at 200 °C for 40 min. Then, the mixture was cooled to 120 °C and degassed under vacuum for 30 min. Afterwards, the temperature

was raised to 280 °C under N_2 at a rate of ~15 °C/min. Starting at 200 °C, a solution of 34.7 µL 1-octanethiol (0.2 mmol) dissolved in 3 mL ODE and a solution of 0.5 mL $Zn(OA)_2$ (0.2 M) dissolved in 3 mL ODE were simultaneously injected at a rate of 3 mL/h. After complete injection, 1 mL OA (stored in a N_2-filled glovebox) was injected and the product was cooled down, and, at 40 °C, ~5 mL hexane was added. The core/shell NPLs were purified by selective precipitation as described for 4-monolayer-CdSe/$Cd_xZn_{1-x}S$. The purified core/shell NPLs were stored in the dark under ambient conditions.

Synthesis of CdSe/ZnS Core/Shell NPLs with a Smooth Shell. In a typical synthesis, 4-monolayer CdSe NPLs [an amount equivalent to 1 mL of NPL dispersion with an optical density (OD) of 60 at the lowest energy excitonic peak, assuming a 1-cm optical path length], 5 mL ODE, 200 µL OA, and 31.4 mg $Zn(oleate)_2$ (0.05 mmol) were added to a 50-mL round-bottom flask. The mixture was degassed under vacuum for 35 min at RT and 15 min at 80 °C. Afterwards, 1 mL OAm (stored in a N_2-filled glovebox) was added and the temperature was raised to 300 °C under N_2 at a rate of ~15 °C/min. Starting at 165 °C, a solution of 42 µL 1-octanethiol (0.24 mmol) dissolved in 4 mL ODE and 2 mL OA, and a solution of 0.75 mL $Zn(OA)_2$ (0.2 M) dissolved in 6 mL ODE were injected simultaneously at a rate of 3 mL/h. After complete injection, the solution was kept at 300 °C for 30 min. Subsequently, the product was cooled down, and, at 40 °C, ~2 mL hexane was added. The core/shell NPLs were purified by selective precipitation. In a first step, 5 mL methyl acetate was added and the mixture was centrifuged at 6500 rpm (5668 g) for 10 min. The core/shell NPLs in the precipitate were re-dispersed in 4 mL hexane. [If a significant amount of core/shell NPLs remained in the supernatant after this centrifugation step, they can be precipitated by adding methyl acetate and centrifuging at 6500 rpm (5668 g).] Then, the dispersion was centrifuged at 6500 rpm (5668 g) for 10 min to remove side products and unreacted precursors. The core/shell NPLs in the supernatant were then precipitated from the hexane dispersion by adding ~5 mL methyl acetate and centrifuging at 6500 rpm (5668 g) for 10 min. This precipitation process was repeated. The core/shell NPLs were then re-dispersed in 3 mL hexane and centrifuged at 6500 rpm (5668 g) for 7 min to separate the stable core/shell NPLs in the supernatant from aggregated core/shell NPLs. The core/shell NPLs in the supernatant were then filtered using a 0.2 µm pore-size PTFE filter and stored in the dark under ambient conditions.

Synthesis of CdSe/ZnSe Core/Shell NPLs. In a typical synthesis, 4-monolayer CdSe NPLs [an amount equivalent to 1 mL of NPL dispersion with an optical density (OD) of 60 at the lowest energy excitonic peak, assuming a 1-cm optical path length], 5 mL ODE, 200 µL OA, and 62.8 mg $Zn(oleate)_2$ (0.1 mmol) were added to a 50-mL round-bottom flask. The mixture was degassed under vacuum for 35 min at RT and 15 min at 80 °C. Afterwards, 1 mL OAm (stored in a N_2-filled glovebox) was added and the temperature was raised to 300 °C under N_2 at a rate of ~15 °C/min. Starting at 165 °C, a solution of 1 mL Se-ODE stock solution dissolved in 3 mL ODE and 2 mL OA was injected

at a rate of 3 mL/h. After complete injection, the solution was kept at 300 °C for 30 min. Subsequently, the product was cooled down, and, at 50 °C, ~2 mL hexane was added. The core/shell NPLs were purified by selective precipitation. In a first step, methyl acetate was added until the mixture turned turbid, and it was centrifuged at 6500 rpm (5668 g) for 10 min. The core/shell NPLs in the precipitate were re-dispersed in 4 mL hexane and precipitated by adding ~5 mL methyl acetate and centrifuging at 6500 rpm (5668 g) for 10 min. This precipitation process was repeated. The core/shell NPLs were then re-dispersed in 3 mL hexane and centrifuged at 6500 rpm (5668 g) for 7 min to separate the stable core/shell NPLs in the supernatant from aggregated core/shell NPLs. The core/shell NPLs in the supernatant were then filtered using a 0.2 μm pore-size PTFE filter and stored in the dark under ambient conditions.

Synthesis of CdSe/$Cd_xZn_{1-x}S$ Core/Shell NPLs with 6-Monolayer-Thick CdSe NPL Cores. In a typical synthesis, 6-monolayer CdSe NPLs [an amount equivalent to 1 mL of NPL dispersion with an optical density (OD) of 20 at the lowest energy excitonic peak, assuming a 1-cm optical path length], 5 mL ODE, 200 μL OA, 45 mg $Cd(oleate)_2$, and 83.8 mg $Zn(oleate)_2$ (total of 0.2 mmol metal oleate, molar ratio of 1:2) were added to a 50-mL round-bottom flask. The mixture was degassed under vacuum for 35 min at RT and 15 min at 80 °C. Afterwards, 1 mL OAm (stored in a N_2-filled glovebox) was added and the temperature was raised to 300 °C under N_2 at a rate of ~15 °C/min. Starting at 165 °C, a solution of 42 μL 1-octanethiol (0.24 mmol) dissolved in 3.5 mL ODE and 1 mL OA was injected at a rate of 2.25 mL/h. After complete injection, the solution was kept at 300 °C for 40 min. Subsequently, the product was cooled down, and, at 40 °C, ~2.5 mL hexane was added. The core/shell NPLs were purified by selective precipitation. In a first step, the mixture was centrifuged at 6500 rpm (5668 g) for 6 min. The core/shell NPLs in the precipitate were re-dispersed in 3 mL hexane. [If a significant amount of core/shell NPLs remained in the supernatant after this centrifugation step, they can be precipitated by adding methyl acetate and centrifuging at 6500 rpm (5668 g).] Then, ~3 mL methyl acetate was added to the dispersion of core/shell NPLs in hexane until the mixture turned turbid, and it was centrifuged at 6500 rpm (5668 g) for 10 min. This process was repeated. The core/shell NPLs were then re-dispersed in 2 mL hexane and centrifuged at 6500 rpm (5668 g) for 7 min to separate the stable core/shell NPLs in the supernatant from aggregated core/shell NPLs. The core/shell NPLs in the supernatant were then filtered using a 0.2 μm pore-size PTFE filter and stored in the dark under ambient conditions.

Fabrication of Core/Shell NPL Ring Resonators. NPL ring resonators were fabricated using the template-stripping technique from Prins et al.[56] to obtain ring structures as described by le Feber et al.[55] In a first step, silicon (100) templates were patterned using electron-beam lithography (Vistec, EBGP 520) and subsequent inductive plasma deep reactive-ion etching (Oxford, Plasmalab System 100). To facilitate stripping of the NPL films, the silicon templates were functionalized with a self-assembled monolayer of octadecyltrichlorosilane. Uniform films of NPLs were then deposited by

drop-casting 35 μL of NPL dispersions in a hexane:octane mixture of 9:1. Template stripping was then performed by attaching a glass slide to the deposited NPL film with an epoxy glue (Norland Products, NOA 61) and curing it under a 365-nm ultraviolet lamp. The NPL-film/epoxy/glass stack was then removed from the silicon template by stripping it off with a razor blade. Subsequently, the Si template was cleaned by ultra-sonication in chloroform for 5 min for re-use.

Absorbance. Optical absorption spectra for ultraviolet to visible wavelengths (UV-Vis) were collected using a Varian Cary 50 spectrometer. The measurements were performed by diluting the samples in hexane and using 1-cm path-length quartz cuvettes.

Photoluminescence (PL) and Photoluminescence Decays. PL spectra were recorded at RT using an Edinburgh Instruments FLS 980 fluorometer. For the standard PL spectra presented in this work, the excitation wavelength was set to 400 nm. The excitation-emission maps shown in Figure S11 were recorded using excitation wavelengths spaced by 5 nm. For photoluminescence decays, the photoluminescence-lifetime capability of the same fluorometer was used. A pulsed laser diode at 373 nm with a repetition rate of 100 kHz and a pulse duration of ~65 ps was used as the excitation source. The detected wavelength was set to the peak emission wavelength for the various core- and core/shell NPLs. The detector was the same cooled Hamamatsu R928P photomultiplier tube used to collect the PL results.

Photoluminescence Quantum Yield (QY). QY values were measured at RT using a Hamamatsu C11347 Quantaurus-QY spectrometer equipped with an integrating sphere. QY values were obtained for different excitation wavelengths from 370 nm to the emission onset in 10-nm steps or by performing single measurements exciting the samples at 400 nm. Unless stated, single QY values reported in the main text and the Supporting Information are obtained by exciting at 400 nm. The measurements were performed after NPL purification by diluting the samples in hexane and using quartz cuvettes with a 1-cm path length. The cuvettes were cleaned in a 1%-solution of Hellmanex™ III after QY measurements to ensure accurate results. The measurement uncertainty is <5% (for Rhodamine 6G in ethanol we measured a QY of 91%).

Transmission Electron Microscopy (TEM), Scanning Transmission Electron Microscopy (STEM), and Energy Dispersive X-ray Spectroscopy (EDS). TEM, STEM, and EDS were performed using an FEI Talos F200X electron microscope operated at 200 kV. The samples were prepared by drop-casting nanocrystals dispersed in hexane on carbon-coated copper grids. The EDS image resolution is ~1 nm.

Atomic-resolution images were acquired with a JEOL JEM-ARM300F Grand ARM microscope operated at 300 kV. The sample was prepared by drop-casting nanocrystals dispersed in hexane on silicon dioxide support films.

Powder X-ray Diffraction (XRD). XRD measurements were performed using a Bruker D2 Phaser instrument (30 kV, 10 mA, $\lambda_{CuK\alpha}$ = 1.54184 Å). The samples were drop-casted from highly concentrated hexane dispersions onto zero-background Si holders.

Nanoplatelet Ring Lasers. Laser experiments were performed using a 405-nm pulsed excitation (~340 fs pulse duration, 10 kHz repetition rate), generated by a collinear optical parametric amplifier (Spectra-Physics, Spirit OPA) pumped by a 1040-nm laser (Spectra-Physics, Spirit 1040-8). To detect the emission signal, an inverted microscope (Nikon, Eclipse Ti-U) with a 50x air objective (Nikon, 0.8 numerical aperture) was used. The beam was directed to the sample through a dichroic beamsplitter (488-nm long pass, AHV, Analysentechnik). The emission was collected by the same objective and directed through a 503-nm long-pass emission filter (AHF, Analysentechnik) into a spectrometer (Andor, Shamrock 303i). Spectra were obtained by dispersing the emission with a 300 lines/mm grating (500 nm blaze), and detecting the output with a complementary metal oxide semiconductor (CMOS) camera (Andor, Zyla 4.2 Plus). The measurements were performed under ambient conditions and analyzed as reported by le Feber et al.[55]

ASSOCIATED CONTENT

Supporting Information

The Supporting Information is available free of charge on the ACS Publications website at DOI: 10.1021/

Additional descriptions of synthetic protocols and the NPL size and shape evaluation, Figures S1–S14, providing additional optical spectra, electron micrographs, EDS, RBS, laser power curves, and the NPL size/shape analysis.

AUTHOR INFORMATION

Corresponding Author

*Email: dnorris@ethz.ch.

ORCID

Aurelio A. Rossinelli: 0000-0001-6930-4190

Henar Rojo: 0000-0003-1543-6264

Aniket S. Mule: 0000-0001-8387-080X

Marianne Aellen: 0000-0003-1548-0433

Ario Cocina: 0000-0003-1560-5849

Eva De Leo: 0000-0002-9677-0274

Robin Schäublin: 0000-0002-8379-9705

David J. Norris: 0000-0002-3765-0678

Notes

The authors declare no competing financial interest.

ACKNOWLEDGMENTS

This work was supported by the Swiss National Science Foundation under Grant No. 200021-165559, and the European Research Council under the European Union's Seventh Framework Program (FP/2007-2013) / ERC Grant Agreement No. 339905 (QuaDoPS Advanced Grant). We thank M. Döbeli and S. Pratsinis for assistance with RBS and XRD, respectively, P. Guyot-Sionnest, F. Knüsel, S. Mazzotti, and M. Wörle for stimulating discussions, A. Riedinger and P. Kumar for reading the manuscript, and S. Meyer for technical assistance. We utilized facilities at the Scientific Center for Optical and Electronic Microscopy (ScopeM) and the Laboratory of Ion Beam Physics at ETH Zurich.

REFERENCES

1. J. Owen; L. Brus, Chemical Synthesis and Luminescence Applications of Colloidal Semiconductor Quantum Dots. *J. Am. Chem. Soc.* **2017**, *139*, 10939–10943.

2. Y. Shirasaki; G. J. Supran; M. G. Bawendi; V. Bulović, Emergence of Colloidal Quantum-Dot Light-Emitting Technologies. *Nat. Photon.* **2012**, *7*, 13–23.
3. Y. E. Panfil; M. Oded; U. Banin, Colloidal Quantum Nanostructures: Emerging Materials for Display Applications. *Angew. Chem. Int. Ed.* **2018**, *57*, 4274–4295.
4. J. Lim; Y.-S. Park; V. I. Klimov, Optical Gain in Colloidal Quantum Dots Achieved with Direct-Current Electrical Pumping. *Nat. Mater.* **2018**, *17*, 42–49.
5. Y. Wang; I. Fedin; H. Zhang; D. V. Talapin, Direct Optical Lithography of Functional Inorganic Nanomaterials. *Science* **2017**, *357*, 385–388.
6. P. Reiss; M. Protière; L. Li, Core/Shell Semiconductor Nanocrystals. *Small* **2009**, *5*, 154–168.
7. S. Ithurria; B. Dubertret, Quasi 2D Colloidal CdSe Platelets with Thicknesses Controlled at the Atomic Level. *J. Am. Chem. Soc.* **2008**, *130*, 16504–16505.
8. A. Riedinger; F. D. Ott; A. Mule; S. Mazzotti; P. N. Knüsel; S. J. P. Kress; F. Prins; S. C. Erwin; D. J. Norris, An Intrinsic Growth Instability in Isotropic Materials Leads to Quasi-Two-Dimensional Nanoplatelets. *Nat. Mater.* **2017**, *16*, 743–748.
9. S. Ithurria; M. D. Tessier; B. Mahler; R. P. S. M. Lobo; B. Dubertret; A. L. Efros, Colloidal Nanoplatelets with Two-Dimensional Electronic Structure. *Nat. Mater.* **2011**, *10*, 936–941.
10. F. Rajadell; J. I. Climente; J. Planelles, Excitons in Core–Only, Core–Shell and Core–Crown CdSe Nanoplatelets: Interplay Between In-Plane Electron–Hole Correlation, Spatial Confinement, and Dielectric Confinement. *Phys. Rev. B* **2017**, *96*, 035307.
11. M. Pelton, Carrier Dynamics, Optical Gain, and Lasing with Colloidal Quantum Wells. *J. Phys. Chem. C* **2018**, *122*, 10659–10674.
12. F. Zhang; S. Wang; L. Wang; Q. Lin; H. Shen; W. Cao; C. Yang; H. Wang; L. Yu; Z. Du; J. Xue; L. S. Li, Super Color Purity Green Quantum Dot Light-Emitting Diodes Fabricated by Using CdSe/CdS Nanoplatelets. *Nanoscale* **2016**, *8*, 12182–12188.
13. S. J. Lim; W. Kim; S. K. Shin, Surface-Dependent, Ligand-Mediated Photochemical Etching of CdSe Nanoplatelets. *J. Am. Chem. Soc.* **2012**, *134*, 7576–7579.
14. M. Olutas; B. Guzelturk; Y. Kelestemur; A. Yeltik; S. Delikanli; H. V. Demir, Lateral Size-Dependent Spontaneous and Stimulated Emission Properties in Colloidal CdSe Nanoplatelets. *ACS Nano* **2015**, *9*, 5041–5050.
15. S. Singh; R. Tomar; S. ten Brinck; J. De Roo; P. Geiregat; J. C. Martins; I. Infante; Z. Hens, Colloidal CdSe Nanoplatelets, a Model for Surface Chemistry/Optoelectronic Property Relations in Semiconductor Canocrystals. *J. Am. Chem. Soc.* **2018**, *140*, 13292–13300.
16. O. Chen; J. Zhao; V. P. Chauhan; J. Cui; C. Wong; D. K. Harris; H. Wei; H.-S. Han; D. Fukumura; R. K. Jain; M. G. Bawendi, Compact High-Quality CdSe–CdS Core–Shell Nanocrystals with Narrow Emission Linewidths and Suppressed Blinking. *Nat. Mater.* **2013**, *12*, 445–451.

17. K. Boldt; N. Kirkwood; G. A. Beane; P. Mulvaney, Synthesis of Highly Luminescent and Photo-Stable, Graded Shell CdSe/$Cd_xZn_{1-x}S$ Nanoparticles by in Situ Alloying. *Chem. Mater.* **2013**, *25*, 4731–4738.
18. Y. Wang; K. E. Fong; S. Yang; Van D. Ta; Y. Gao; Z. Wang; V. Nalla; H. V. Demir; H. Sun, Unraveling the Ultralow Threshold Stimulated Emission from CdZnS/ZnS Quantum Dot and Enabling High-Q Microlasers. *Laser Photonics Rev.* **2015**, *9*, 507–516.
19. F. D. Ott; A. Riedinger; D. R. Ochsenbein; P. N. Knüsel; S. C. Erwin; M. Mazzotti; D. J. Norris, Ripening of Semiconductor Nanoplatelets. *Nano Lett.* **2017**, *17*, 6870–6877.
20. S. Ithurria; D. V. Talapin, Colloidal Atomic Layer Deposition (c-ALD) Using Self-Limiting Reactions at Nanocrystal Surface Coupled to Phase Transfer Between Polar and Nonpolar Media. *J. Am. Chem. Soc.* **2012**, *134*, 18585–18590.
21. Y. Kelestemur; B. Guzelturk; O. Erdem; M. Olutas; K. Gungor; H. V. Demir, Platelet-In-Box Colloidal Quantum Wells: CdSe/CdS@CdS Core/Crown@Shell Heteronanoplatelets. *Adv. Funct. Mater.* **2016**, *26*, 3570–3579.
22. B. Mahler; B. Nadal; C. Bouet; G. Patriarche; B. Dubertret, Core/Shell Colloidal Semiconductor Nanoplatelets. *J. Am. Chem. Soc.* **2012**, *134*, 18591–18598.
23. M. D. Tessier; B. Mahler; B. Nadal; H. Heuclin; S. Pedetti; B. Dubertret, Spectroscopy of Colloidal Semiconductor Core/Shell Nanoplatelets with High Quantum Yield. *Nano Lett.* **2013**, *13*, 3321–3328.
24. A. Polovitsyn; Z. Dang; J. L. Movilla; B. Martín-García; A. H. Khan; G. H. V. Bertrand; R. Brescia; I. Moreels, Synthesis of Air-Stable CdSe/ZnS Core–Shell Nanoplatelets with Tunable Emission Wavelength. *Chem. Mater.* **2017**, *29*, 5671–5680.
25. A. A. Rossinelli; A. Riedinger; P. Marqués-Gallego; P. N. Knüsel; F. V. Antolinez; D. J. Norris, High-Temperature Growth of Thick-Shell CdSe/CdS Core/Shell Nanoplatelets. *Chem. Commun.* **2017**, *53*, 9938–9941.
26. F. Feng; L. T. Nguyen; M. Nasilowski; B. Nadal; B. Dubertret; A. Maître; L. Coolen, Probing the Fluorescence Dipoles of Single Cubic CdSe/CdS Nanoplatelets with Vertical or Horizontal Orientations. *ACS Photonics* **2018**, *5*, 1994–1999.
27. M. A. Hines; P. Guyot-Sionnest, Synthesis and Characterization of Strongly Luminescing ZnS-Capped CdSe Nanocrystals. *J. Phys. Chem.* **1996**, *100*, 468–471.
28. X. Peng; M. C. Schlamp; A. V. Kadavanich; A. P. Alivisatos, Epitaxial Growth of Highly Luminescent CdSe/CdS Core/Shell Nanocrystals with Photostability and Electronic Accessibility. *J. Am. Chem. Soc.* **1997**, *119*, 7019–7029.
29. B. O. Dabbousi; J. Rodriguez-Viejo; F. V. Mikulec; J. R. Heine; H. Mattoussi; R. Ober; K. F. Jensen; M. G. Bawendi, (CdSe)ZnS Core−Shell Quantum Dots: Synthesis and Characterization

of a Size Series of Highly Luminescent Nanocrystallites. *J. Phys. Chem. B* **1997**, *101*, 9463–9475.

30. H. Cruguel; C. Livache; B. Martinez; S. Pedetti; D. Pierucci; E. Izquierdo; M. Dufour; S. Ithurria; H. Aubin; A. Ouerghi; E. Lacaze; M. G. Silly; B. Dubertret; E. Lhuillier, Electronic Structure of CdSe–ZnS 2D Nanoplatelets. *Appl. Phys. Lett.* **2017**, *110*, 152103.
31. Y. Altintas; U. Quliyeva; K. Gungor; O. Erdem; Y. Kelestemur; E. Mutlugun; M. V. Kovalenko; H. V. Demir, Highly Stable, Near-Unity Efficiency Atomically Flat Semiconductor Nanocrystals of CdSe/ZnS Hetero-Nanoplatelets Enabled by ZnS-Shell Hot-Injection Growth. *Small* **2019**, *15*, 1804854.
32. Z.-J. Jiang; D. F. Kelley, Stranski–Krastanov Shell Growth in ZnTe/CdSe Core/Shell Nanocrystals. *J. Phys. Chem. C* **2013**, *117*, 6826–6834.
33. S. G. Kwon; G. Krylova; P. J. Phillips; R. F. Klie; S. Chattopadhyay; T. Shibata; E. E. Bunel; Y. Liu; V. B. Prakapenka; B. Lee; E. V. Shevchenko, Heterogeneous Nucleation and Shape Transformation of Multicomponent Metallic Nanostructures. *Nat. Mater.* **2015**, *14*, 215–223.
34. B. Ji; Y. E. Panfil; N. Waiskopf; S. Remennik; I. Popov; U. Banin, Strain-Controlled Shell Morphology on Quantum Rods. *Nat. Commun.* **2019**, *10*, 2.
35. S. Abe; R. K. Capek; B. De Geyter; Z. Hens, Reaction Chemistry/Nanocrystal Property Relations in the Hot Injection Synthesis, the Role of the Solute Solubility. *ACS Nano* **2013**, *7*, 943–949.
36. D. Shaw, Diffusion Mechanisms in II–VI Materials. *J. Cryst. Growth* **1988**, *86*, 778–796.
37. N. Oh; M. Shim, Metal Oleate Induced Etching and Growth of Semiconductor Nanocrystals, Nanorods, and Their Heterostructures. *J. Am. Chem. Soc.* **2016**, *138*, 10444–10451.
38. R. Xie; U. Kolb; J. Li; T. Basché; A. Mews, Synthesis and Characterization of Highly Luminescent CdSe−Core CdS/$Zn_{0.5}Cd_{0.5}$S/ZnS Multishell Nanocrystals. *J. Am. Chem. Soc.* **2005**, *127*, 7480–7488.
39. L. Manna; E. C. Scher; L.-S. Li; A. P. Alivisatos, Epitaxial Growth and Photochemical Annealing of Graded CdS/ZnS Shells on Colloidal CdSe Nanorods. *J. Am. Chem. Soc.* **2002**, *124*, 7136–7145.
40. I. Nakonechnyi; M. Sluydts; Y. Justo; J. Jasieniak; Z. Hens, Mechanistic Insights in Seeded Growth Synthesis of Colloidal Core/Shell Quantum Dots. *Chem. Mater.* **2017**, *29*, 4719–4727.
41. B. M. Saidzhonov; V. F. Kozlovsky; V. B. Zaytsev; R. B. Vasiliev, Ultrathin CdSe/CdS and CdSe/ZnS Core–Shell Nanoplatelets: The Impact of the Shell Material on the Structure and Optical Properties. *J. Lumin.* **2019**, *209*, 170–178.
42. J. Cui; A. P. Beyler; I. Coropceanu; L. Cleary; T. R. Avila; Y. Chen; J. M. Cordero; S. L. Heathcote; D. K. Harris; O. Chen; J. Cao; M. G. Bawendi, Evolution of the Single-Nanocrystal

Photoluminescence Linewidth with Size and Shell: Implications for Exciton–Phonon Coupling and the Optimization of Spectral Linewidths. *Nano Lett.* **2016**, *16*, 289–296.

43. N. Tschirner; H. Lange; A. Schliwa; A. Biermann; C. Thomsen; K. Lambert; R. Gomes; Z. Hens, Interfacial Alloying in CdSe/CdS Heteronanocrystals: A Raman Spectroscopy Analysis. *Chem. Mater.* **2012**, *24*, 311–318.
44. A. Rubin-Brusilovski; Y. Jang; A. Shapiro; A. Safran; A. Sashchiuk; E. Lifshitz, Influence of Interfacial Strain on Optical Properties of PbSe/PbS Colloidal Quantum Dots. *Chem. Mater.* **2016**, *28*, 9056–9063.
45. I. Coropceanu; A. Rossinelli; J. R. Caram; F. S. Freyria; M. G. Bawendi, Slow-Injection Growth of Seeded CdSe/CdS Nanorods with Unity Fluorescence Quantum Yield and Complete Shell to Core Energy Transfer. *ACS Nano* **2016**, *10*, 3295–3301.
46. S. Christodoulou; J. I. Climente; J. Planelles; R. Brescia; M. Prato; B. Martín-García; A. H. Khan; I. Moreels, Chloride-Induced Thickness Control in CdSe Nanoplatelets. *Nano Lett.* **2018**, *18*, 6248–6254.
47. W. Cho; S. Kim; I. Coropceanu; V. Srivastava; B. T. Diroll; A. Hazarika; I. Fedin; G. Galli; R. D. Schaller; D. V. Talapin, Direct Synthesis of Six-Monolayer (1.9 nm) Thick Zinc-Blende CdSe Nanoplatelets Emitting at 585 nm. *Chem. Mater.* **2018**, *30*, 6957–6960.
48. V. I. Klimov; A. A. Mikhailovsky; D. W. McBranch; C. A. Leatherdale; M. G. Bawendi, Quantization of Multiparticle Auger Rates in Semiconductor Quantum Dots. *Science* **2000**, *287*, 1011–1013.
49. G. E. Cragg; A. L. Efros, Suppression of Auger Processes in Confined Structures. *Nano Lett.* **2010**, *10*, 313–317.
50. G. A. Beane; K. Gong; D. F. Kelley, Auger and Carrier Trapping Dynamics in Core/Shell Quantum Dots Having Sharp and Alloyed Interfaces. *ACS Nano* **2016**, *10*, 3755–3765.
51. C. She; I. Fedin; D. S. Dolzhnikov; A. Demortière; R. D. Schaller; M. Pelton; D. V. Talapin, Low-Threshold Stimulated Emission Using Colloidal Quantum Wells. *Nano Lett.* **2014**, *14*, 2772–2777.
52. J. Q. Grim; S. Christodoulou; F. Di Stasio; R. Krahne; R. Cingolani; L. Manna; I. Moreels, Continuous-Wave Biexciton Lasing at Room Temperature Using Solution-Processed Quantum Wells. *Nat. Nanotechnol.* **2014**, *9*, 891–895.
53. C. She; I. Fedin; D. S. Dolzhnikov; P. D. Dahlberg; G. S. Engel; R. D. Schaller; D. V. Talapin, Red, Yellow, Green, and Blue Amplified Spontaneous Emission and Lasing Using Colloidal CdSe Nanoplatelets. *ACS Nano* **2015**, *9*, 9475–9485.
54. Z. Yang; M. Pelton; I. Fedin; D. V. Talapin; E. Waks, A Room Temperature Continuous-Wave Nanolaser Using Colloidal Quantum Wells. *Nat. Commun.* **2017**, *8*, 143.

55. B. le Feber; F. Prins; E. De Leo; F. T. Rabouw; D. J. Norris, Colloidal-Quantum-Dot Ring Lasers with Active Color Control. *Nano Lett.* **2018**, *18*, 1028–1034.
56. F. Prins; D. K. Kim; J. Cui; E. De Leo; L. L. Spiegel; K. M. McPeak; D. J. Norris, Direct Patterning of Colloidal Quantum-Dot Thin Films for Enhanced and Spectrally Selective Out-Coupling of Emission. *Nano Lett.* **2017**, *17*, 1319–1325.
57. Y. Altintas; K. Gungor; Y. Gao; M. Sak; U. Quliyeva; G. Bappi; E. Mutlugun; E. H. Sargent; H. V. Demir, Giant Alloyed Hot-Injection Shells Enable Ultralow Optical Gain Threshold in Colloidal Quantum Wells. *ACS Nano* **2019**, *13*, 10662–10670.
58. B. Liu; Y. Altintas; L. Wang; S. Shendre; M. Sharma; H. Sun; E. Mutlugun; H. V. Demir, Record High External Quantum Efficiency of 19.2% Achieved in Light-Emitting Diodes of Colloidal Quantum Wells Enabled by Hot-Injection Shell Growth. *ChemRxiv* **2019**, DOI: 10.26434/chemrxiv.9777632.v1.
59. M. P. Hendricks; M. P. Campos; G. T. Cleveland; I. Jen-La Plante; J. S. Owen, A Tunable Library of Substituted Thiourea Precursors to Metal Sulfide Nanocrystals. *Science* **2015**, *348*, 1226–1230.

TABLES

Material	Emission Peak [nm]	FWHM [meV]	FWHM [nm]	QY [%]	τ_{avg} [ns]
4-monolayer-CdSe/$Cd_xZn_{1-x}S$	655	56	19.5	88	25
6-monolayer-CdSe/$Cd_xZn_{1-x}S$	692	57	22.1	92	22
CdSe/CdS/ZnS	662	67	23.6	78	37
CdSe/ZnS (uniform)	620	76	23.7	52	10
CdSe/ZnS (rough)	612	101	30.7	67	21
CdSe/ZnSe	684	59	22.1	47	13

τ_{avg}: average lifetime

Table 1. Summary of the room-temperature optical properties for the core/shell NPLs presented in Figures 1–9 in the main text. The columns describe the peak wavelength of the emission, its full-width-at-half-maximum (FWHM) in meV and nm, respectively, photoluminescence quantum yield (QY), and average photoluminescence decay time, τ_{avg}.

FIGURES

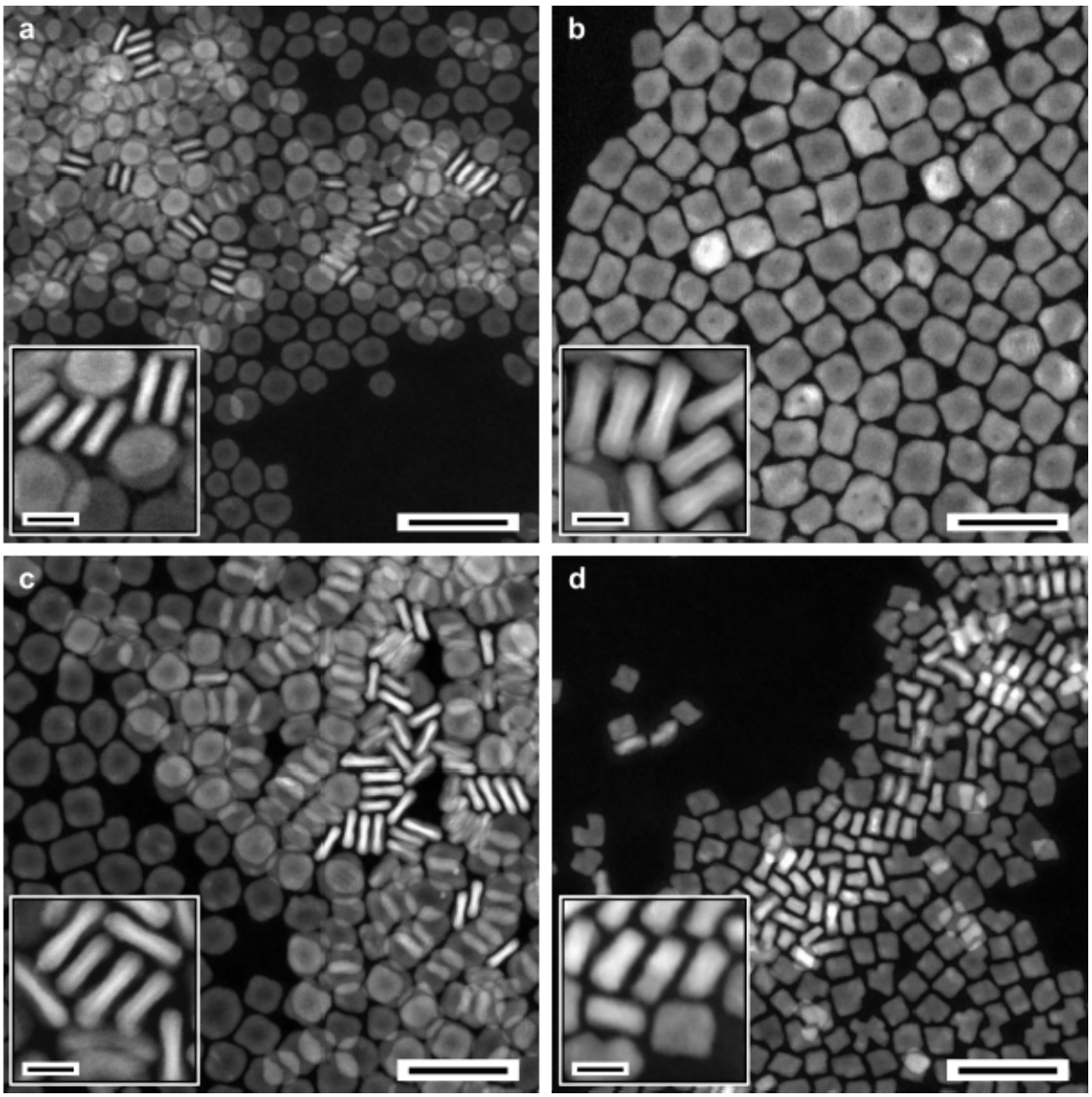

Figure 1. High-angle annular dark-field scanning transmission electron microscopy (HAADF STEM) images of (a) CdSe/ZnS, (b) CdSe/CdS/ZnS, (c) CdSe/$Cd_xZn_{1-x}S$, and (d) CdSe/ZnSe NPLs. All of the NPL cores are 4-monolayers thick. The insets show the corresponding NPLs at higher magnification. Black scale bars are 50 and 10 nm for the large and inset images, respectively.

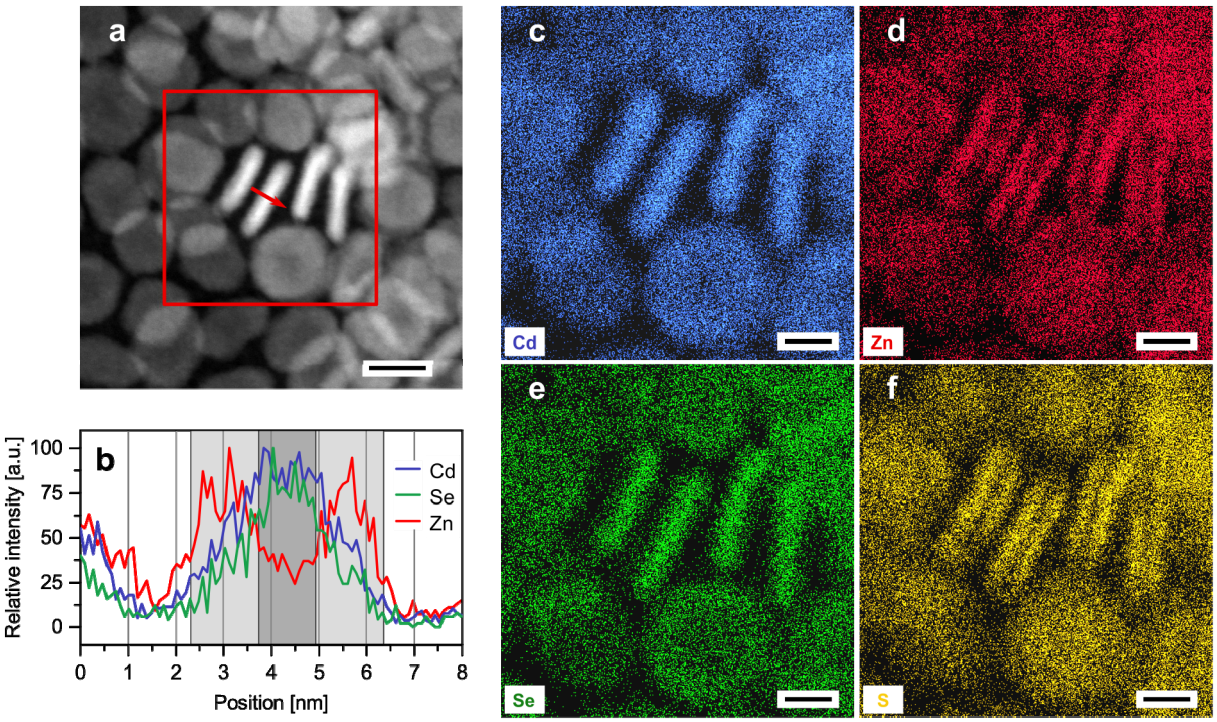

Figure 2. Structural analysis of CdSe/ZnS core/shell NPLs with a uniform shell. The NPL cores are 4-monolayers thick. (a) HAADF STEM image. (b) Cd, Se, and Zn concentration profile across a single CdSe/ZnS NPL from energy dispersive X-ray spectroscopy (EDS). The profile is measured on the NPL marked with a red arrow in (a). Dark and light gray-shaded regions indicate the width of the core and shell, respectively. The resolution of the technique is ~1 nm. (c)-(f) EDS images for Cd, Zn, Se, and S. The scanned region is shown as a red box in (a). Scale bars are 10 nm in (a) and 5 nm in (c)-(f).

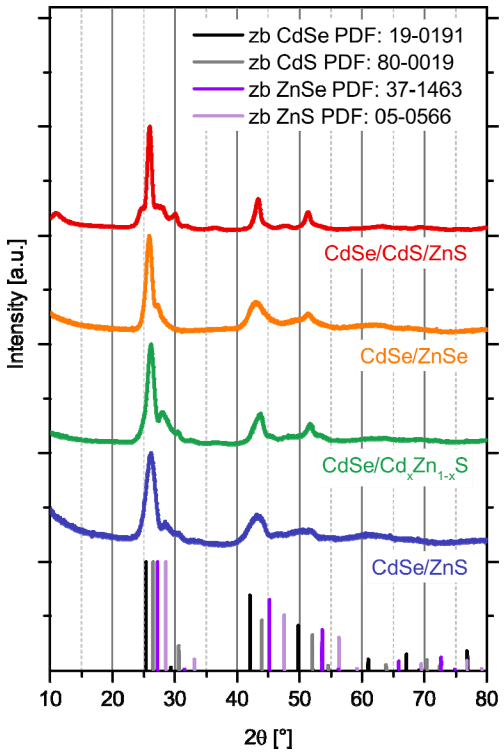

Figure 3. Powder X-ray diffraction (XRD) patterns for the core/shell NPLs shown in Figure 1. All of the NPL cores are 4-monolayers thick. Reference patterns (labelled by their powder diffraction file, PDF) are shown for zinc blende crystals of CdSe, CdS, ZnSe, and ZnS. The XRD pattern for the CdSe NPL cores is shown in Figure S8.

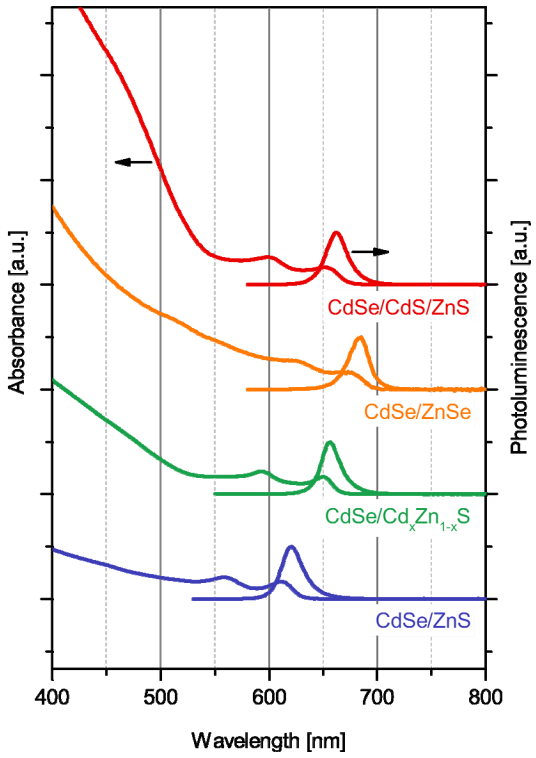

Figure 4. Room-temperature optical absorption and emission spectra for the core/shell NPLs shown in Figure 1. All of the NPL cores are 4-monolayers thick. The emission linewidths range from 56 meV for CdSe/$Cd_xZn_{1-x}S$ to 76 meV for CdSe/ZnS core/shell NPLs (see Table 1 for all parameters). Optical spectra for the CdSe NPL cores are shown in Figure S8.

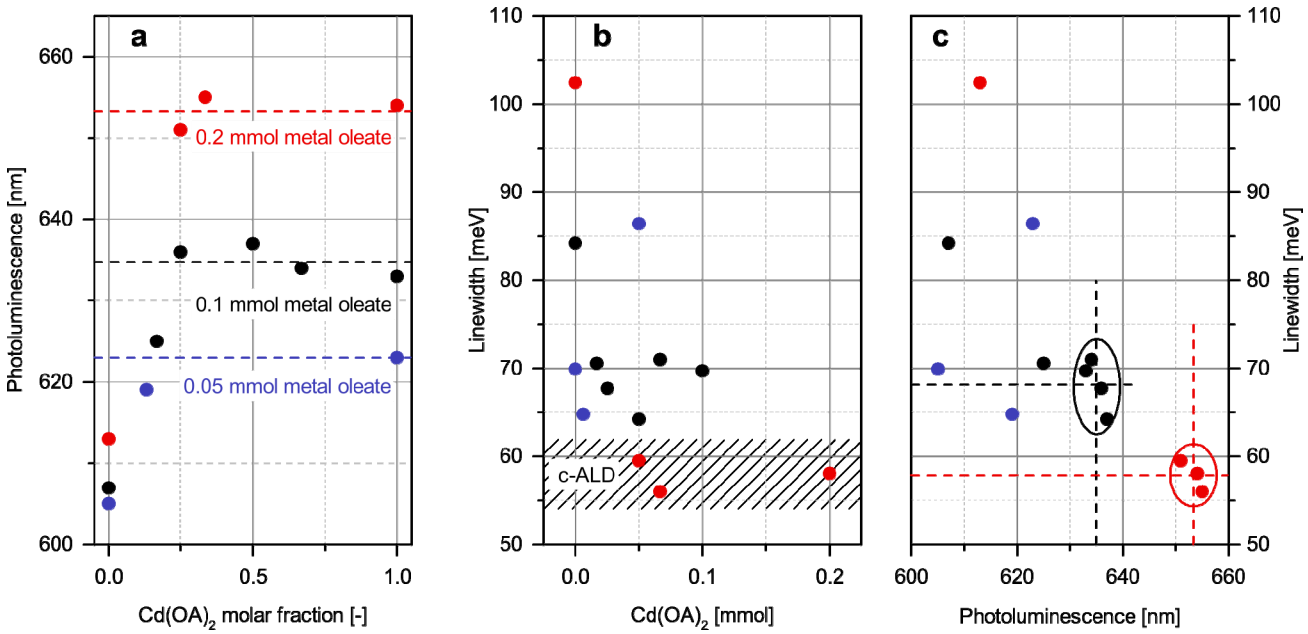

Figure 5. Influence of the precursor ratio and total precursor concentration on the emission properties of $CdSe/Cd_xZn_{1-x}S$ NPLs. All of the NPL cores are 4-monolayers thick. Blue, black, and red dots correspond to reaction series with 0.05, 0.1, and 0.2 mmols of total metal oleate [$Cd(OA)_2$ + $Zn(OA)_2$], respectively. (a) Evolution of the emission wavelength as a function of the $Cd(OA)_2$ molar fraction (relative to the total amount of metal oleate) during the shell growth. (b) Influence of the concentration of $Cd(OA)_2$ on the emission linewidth. The shaded area indicates the linewidth range reported for CdSe/CdS core/shell NPLs synthesized by colloidal atomic layer deposition (c-ALD).[20-21] (c) Relation between the emission wavelength and the corresponding linewidth. The dashed lines indicate the mean photoluminescence wavelengths and linewidths for the reactions using a $Cd(OA)_2$ molar fraction ≥25% [data points inside the circles in (c)].

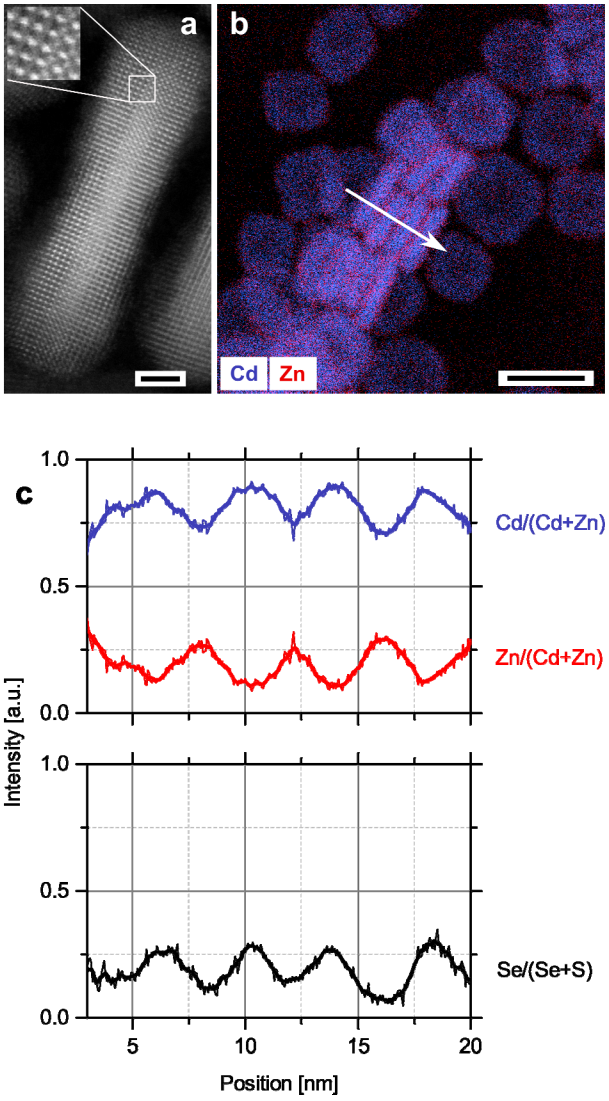

Figure 6. Structural analysis of the CdSe/$Cd_xZn_{1-x}S$ core/shell NPLs shown in Figure 1c. The NPL cores are 4-monolayers thick. (a) High-resolution HAADF STEM cross-sectional image of a single core/shell NPL. The brighter core can be distinguished from the darker shell due to the higher atomic number of the core elements. (b) Superposition of energy-dispersive X-ray spectrographs (EDS) of Cd and Zn for NPLs seen in top- and side-view. (c) The corresponding concentration profile across four vertically stacked NPLs, observed from the side. The collection area is marked with the white arrow in (b). Note that a single core/shell NPL in top-view is detected on the left of the stacked NPLs at positions between 0 and ~7 nm in (c). Black scale bars are 2 nm in (a) and 20 nm in (b).

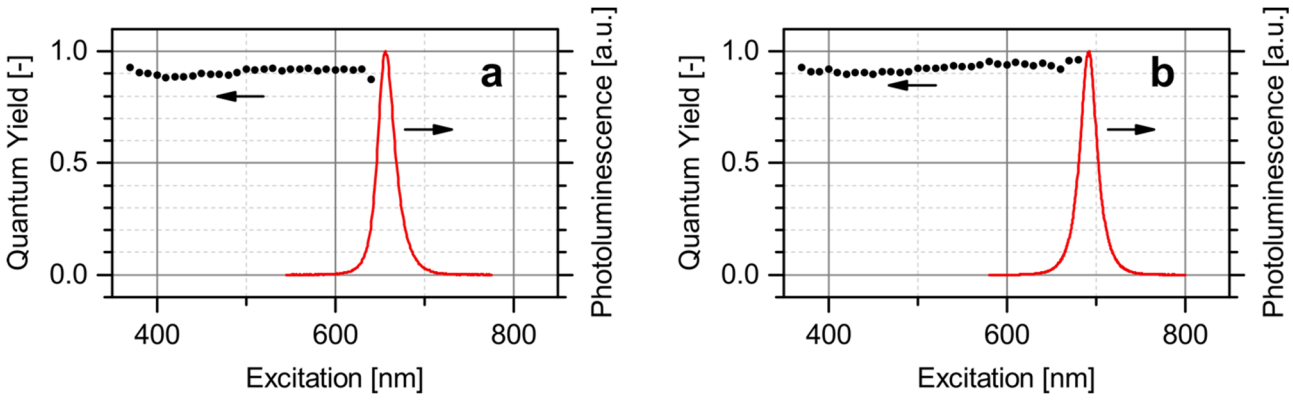

Figure 7. Room-temperature photoluminescence quantum yields (QYs) of CdSe/$Cd_xZn_{1-x}S$ core/shell NPLs having CdSe cores with a thickness of (a) 4 monolayers and (b) 6 monolayers, measured at different excitation wavelengths. The corresponding emission spectra are shown in red.

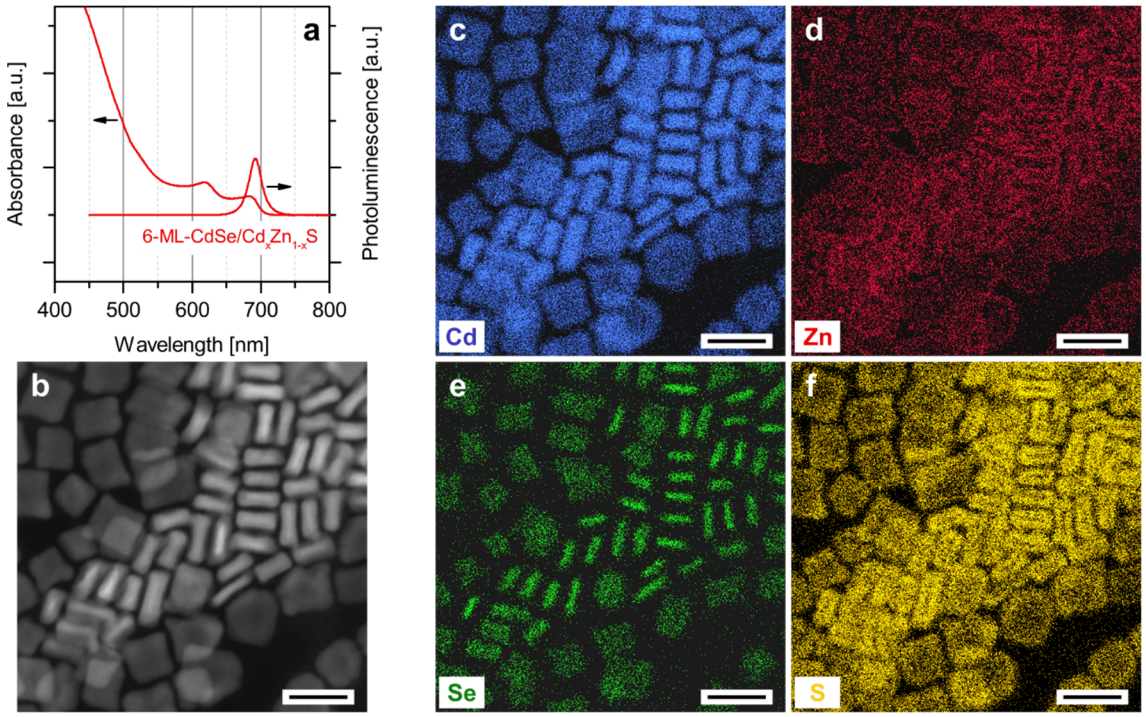

Figure 8. CdSe/$Cd_xZn_{1-x}S$ core/shell NPLs using cores with a thickness of 6 monolayers (6 ML) and a precursor ratio [$Cd(OA)_2$] : [$Zn(OA)_2$] of 1:2. (a) Room-temperature absorption and emission spectra of the core/shell NPLs. (b) HAADF STEM image and (c-f) the corresponding energy dispersive X-ray spectroscopy (EDS) images of Cd, Zn, Se, and S. The resolution of the technique is ~1 nm. Due to the thicker geometry, these core CdSe NPLs show an improved thermal stability and the original rectangular shape is largely preserved in the final core/shell NPL structures. Black scale bars are 20 nm. Optical and STEM data for the 6-monolayer CdSe NPL cores are shown in Figure S12.

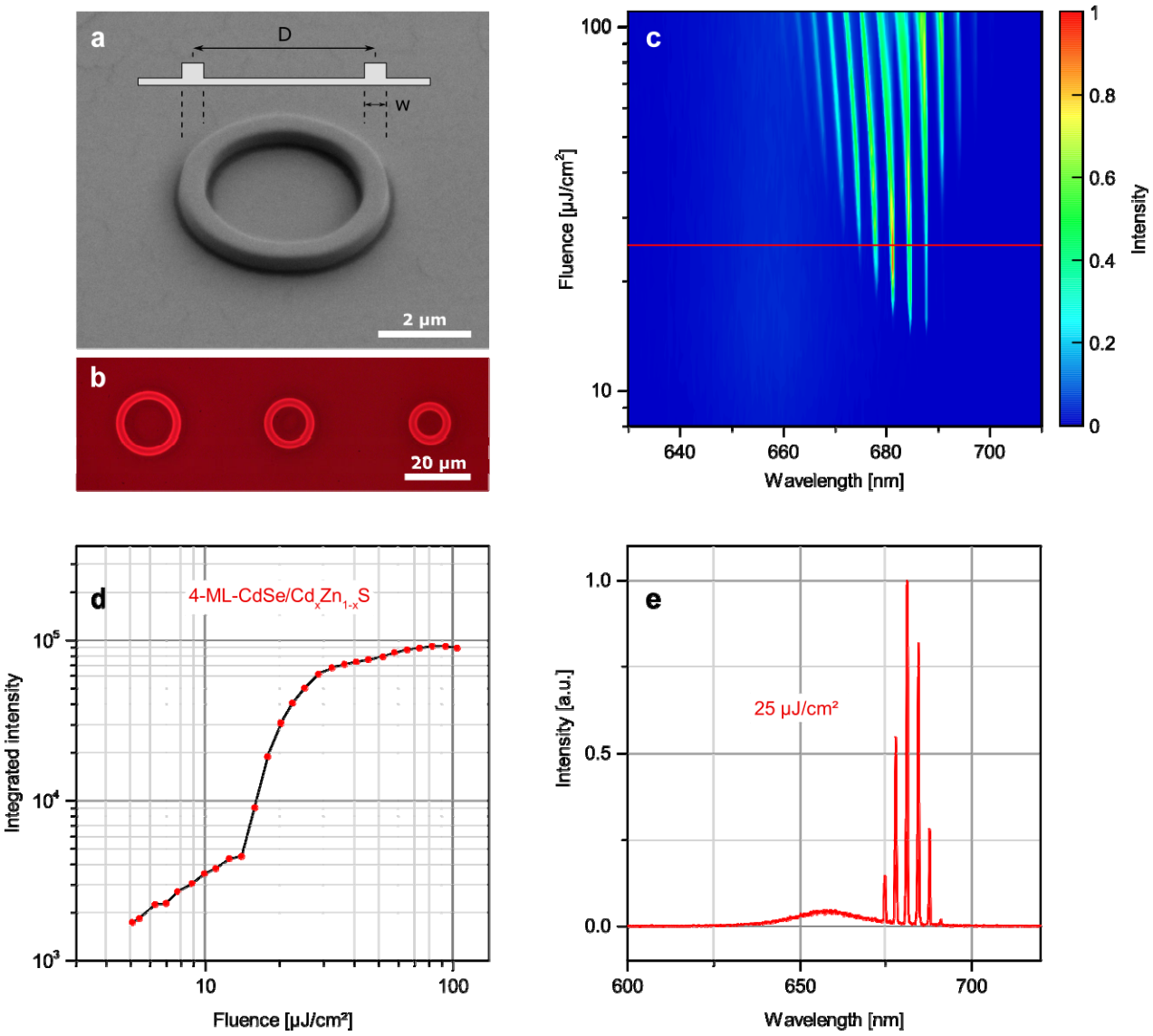

Figure 9. 4-monolayer-CdSe/$Cd_xZn_{1-x}S$ core/shell NPL ring resonators and their optical characterization for lasing. (a) Scanning electron micrograph (SEM) of a template-stripped NPL ring resonator. The inset shows a cross-sectional schematic of the ring structure. Rings were fabricated with variable diameters (D) and widths (w) and a height of ~500 nm. (b) Fluorescence image of ring resonators of varying diameters illuminated with ultraviolet light. (c) Power-dependent emission spectra collected from a ring with D = 20 µm and w = 1 µm. Narrow lasing lines evolve at fluences above a threshold of 13 µJ/cm^2. (d) Corresponding emission intensity integrated over all collected wavelengths and averaged over the area of the ring resonator versus the excitation fluence. (e) Emission spectrum under lasing conditions extracted at a power of 25 µJ/cm^2 [indicated with a red horizontal line in (c)].

TABLE OF CONTENTS GRAPHIC